DM EMI Noise Prediction for Constant On-Time, Critical Mode Power Factor Correction Converters

Zijian Wang, Shuo Wang, *Senior Member, IEEE*, Pengju Kong, *Member, IEEE*, and Fred C. Lee, *Fellow, IEEE*

***Abstract*—Critical conduction mode (CRM) power factor correction (PFC) converters are widely used in industries. For CRM PFC converters, high inductor current ripples generate high differential mode (DM) electromagnetic interference (EMI) noise, which calls for big EMI filters. On the other hand, the switching frequency varies during a half line cycle. The characteristics of the EMI in CRM PFC converters have not been carefully investigated and the worst case DM EMI noise has not been identified. The design of an EMI filter is difficult. In this paper, a mathematical model based on the principle of quasi-peak noise detection is proposed to predict the EMI noise in CRM PFC converters. The developed model is verified by experimental results. Based on this model, the worst case DM EMI noise can be predicted. This will greatly help in the design of EMI filters for CRM PFC converters.**

***Index Terms*—Critical conduction mode (CCM), electromagnetic interference (EMI) noise prediction, mathematical model, quasi-peak detection, worst case analysis.**

I. Introduction

THERE are two popular control modes in power factor correction (PFC) converters: constant-frequency continuous current mode (CCM) and critical conduction mode (CRM). The CRM PFC converter is widely used in power adapters, entry-level servers, and other applications. The biggest advantage of CRM is that the reverse recovery loss of power diodes can almost be eliminated with zero conduction current when MOSFET turns ON. There are two control schemes for CRM PFC: current mode control and voltage mode control. The turn-on time $T_{\rm on}$ of each switching cycle for either mode is constant over a half line cycle to guarantee that the average input current is sinusoidal and it is in phase with the input voltage. Because of the simplicity of voltage mode control, it is becoming more and more popular in CRM PFC converters. In this paper, a CRM PFC converter with voltage mode control is investigated in Fig. 1(a) and (b). In Fig. 1(a), I_L is the current in the boost inductor. When

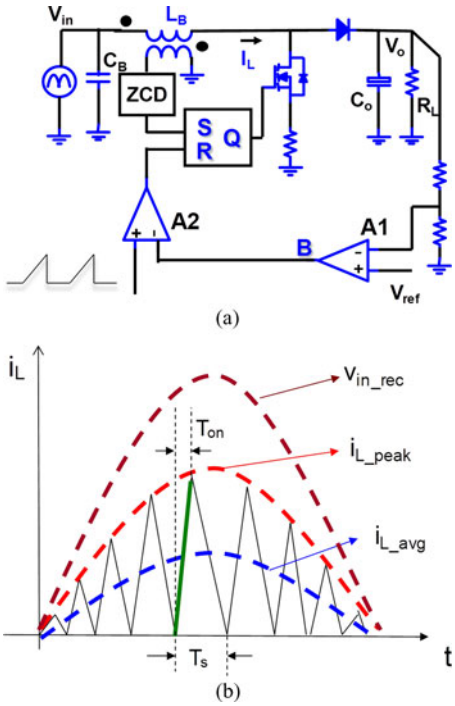

Fig. 1. Voltage mode control scheme for CRM PFC converters. (a) Control scheme. (b) Current and voltage waveforms.

I_L reaches zero, MOSFET is turned ON. The output voltage is sensed and compared with the reference voltage $V_{\rm ref}$. The error voltage V_B is compared with a triangular waveform. When the triangular voltage is higher than V_B, MOSFET is turned OFF. In Fig. 1(b), $V_{\rm in\_rec}$ is the rectified input ac voltage within half line cycle. The diode bridge before the PFC converter is not shown in Fig. 1. $i_{L\,\rm peak}$ is the peak current of I_L. $i_{L\,\rm avg}$ is the average current of I_L. Because the time constant of control loop is much longer than line frequency, on-time $T_{\rm on}$ is almost constant within the half line cycle and given as

$$T_{\rm on} = \frac{2L_B P_o}{\eta V_{\rm RMS}^2}. \tag{1}$$

In (1), P_o is the output power, $V_{\rm RMS}$ is the input RMS voltage, and η is the efficiency.

A major concern for a CRM PFC converter is its high conducted DM EMI noise due to its high inductor current ripple (200% of the average inductor current). Most of the existing literature focus on the EMI noise analysis for constant-frequency CCM PFC converters [1]–[8]. On the other hand, the switching frequency of a CRM PFC converter varies within a half line cycle. This has not been carefully investigated.

Manuscript received January 7, 2011; revised May 26, 2011 and August 2, 2011; accepted December 14, 2011. Date of current version April 3, 2012. Recommended for publication by Associate Editor J.-L. Schanen.

Z. Wang is with Monolithic Power Systems, Inc., San Jose, CA 95120 USA (e-mail: carlwang@vt.edu).

S. Wang is with the Department of Electrical and Computer Engineering, The University of Texas at San Antonio, San Antonio, TX 78249 USA (e-mail: shuowang@ieee.org).

P. Kong is with Intersil Corporation, Milpitas, CA 95035, USA (e-mail: pjkong@vt.edu).

F. C. Lee is with the Department of Electrical and Computer Engineering, Virginia Tech, Blacksburg, VA 24061 USA (e-mail: fclee@vt.edu).

Color versions of one or more of the figures in this paper are available online at http://ieeexplore.ieee.org.

Digital Object Identifier 10.1109/TPEL.2011.2182059

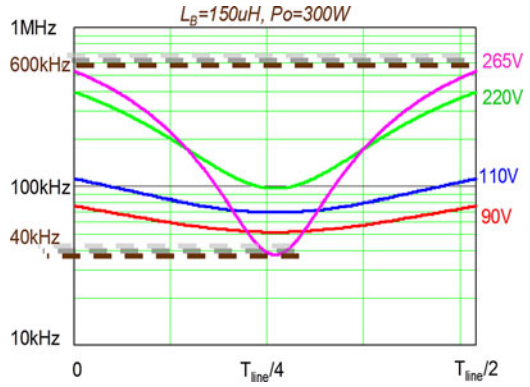

Fig. 2. Switching frequency f_s versus time t at different input line voltages.

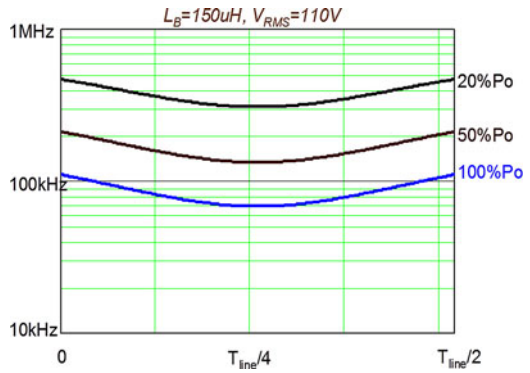

Fig. 3. Switching frequency f_s versus time t at different loads.

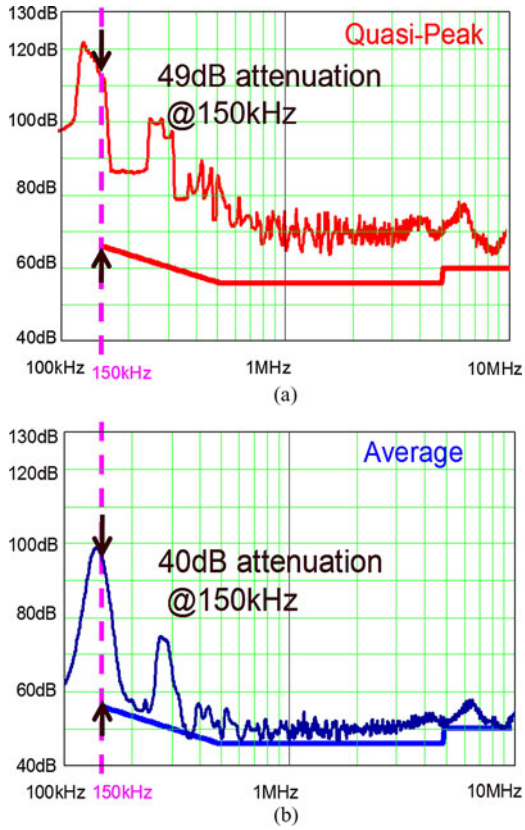

Fig. 4. Comparison of quasi-peak and average noise for a CRM PFC converter. (a) Quasi-peak DM noise. (b) Average DM noise.

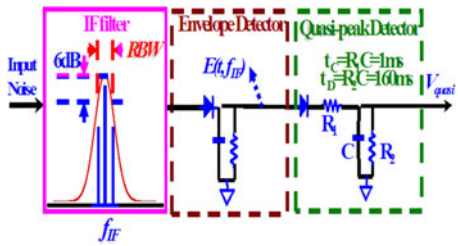

Fig. 5. Block diagram of quasi-peak noise detection.

It is not easy to analyze the EMI of a PFC converter with variable switching frequency. The switching frequency of a CRM PFC converter is a function of time, input line voltage, and load as shown in Figs. 2 and 3. This is quite troublesome because the converter's EMI performance is sensitive to the switching frequencies. In order to design an optimal EMI filter for a CRM PFC converter within whole line voltage and load ranges, the worst EMI noise must be identified.

There is one more special characteristic for the EMI noise in a CRM PFC converter. The comparison between measured quasi-peak DM noise and average DM noise for a CRM PFC converter is shown in Fig. 4. The measurements are carried out at 115 V input and 150 W load. The magnitude of quasi-peak noise is about 20 dB higher than that of average noise. This is related to the frequency modulation effect, which is well explained in [9] and [10]. Since the EMI standards, such as EN55022 [11], of quasi-peak noise are only 10 dB higher than those of average noise, the quasi-peak noise is much more critical than the average noise for a CRM PFC converter. This paper will focus on the prediction of the quasi-peak DM EMI noise. Its result will benefit the EMI filter design for CRM PFC converters.

II. Principle of Quasi-Peak Noise Detection

The principle of quasi-peak noise detection in a classic analog spectrum analyzer is shown in Fig. 5 [13]. There are generally three devices in a quasi-peak detection process: intermediate frequency filter (IF), envelope detector, and quasi-peak detector. IF is a band-pass filter with a 9 kHz resolution bandwidth (RBW) at −6dB. It has an intermediate frequency varying from 150 kHz to 30 MHz. It can be characterized using a near-Gaussian filter.

In this paper, based on the near-Gaussian filter theory, the magnitude of the IF gain is approximately described as

$$|G_{\mathrm{IF}}(f, f_{\mathrm{IF}})| = e^{-(f-f_{\mathrm{IF}})^2/c^2} \tag{2}$$

where f is the frequency of the input noise, f_{IF} is the intermediate frequency, and

$$c = \frac{4.5k}{\sqrt{\ln 2}}. \tag{3}$$

Equation (3) defines the 9 kHz bandwidth at −6dB. A comparison between the IF gains specified in (2) and in the standard is shown in Fig. 6. They match very well.

The input noise signal is first processed through the IF with the IF gain described in (2). Then the envelope detector detects

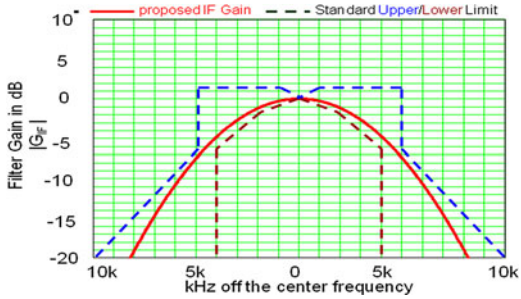

Fig. 6. Comparison between IF gains specified in (2) and the standard.

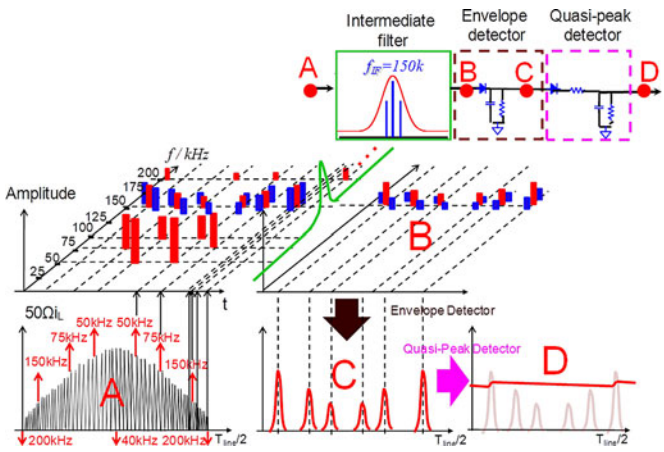

Fig. 7. Principle of quasi-peak DM EMI noise prediction for a CRM PFC converter.

the envelope of the noise signal filtered through the IF. IF and the envelope detector work together to detect the envelope of the noise signal within the band of $f_{\rm IF} \pm 4.5$ kHz and filter out the noise signal outside the RBW. From the mathematical point of view, for the input noise signal with constant frequency f and constant amplitude P, the output of the envelope detector is equal to $P\ |G_{\rm IF}(f, f_{\rm IF})|$. Similarly, for the input noise signal with variable frequency $f(t)$ and variable amplitude $P(t)$, the envelope $E(t, f_{\rm IF})$ would be $P(t)|G_{\rm IF}(f(t), f_{\rm IF})|$. The mathematical models of the output of an envelope detector for any signals can be derived similarly. Finally, the output of the envelope detector is fed to a quasi-peak detector. The quasi-peak detector is a charging and discharging network with time constants specified as [12] charging time constant $\tau_C = 1$ ms and discharging time constant $\tau_D = 160$ ms. The analog circuit for the quasi-peak detector in Fig. 5 is an example of the implementation [14].

Fig. 7 illustrates the detail on how the quasi-peak amplitude of the noise at 150 kHz is predicted for the variable-frequency inductor current in a CRM PFC. It is assumed that the switching frequency ranges from 40 to 200 kHz. The frequencies of the triangular ripple currents which can contribute to the noise at 150 kHz would be 50 kHz (third harmonic), 75 kHz (second harmonic), or 150 kHz (fundamental). The fundamentals and the harmonics of the 50, 75, and 150 kHz triangular current ripples are all shown as red bars in Fig. 7. The heights of the red bars represent the amplitudes of the fundamentals or harmonics. As shown in the figure, only the red bars with frequency equal to

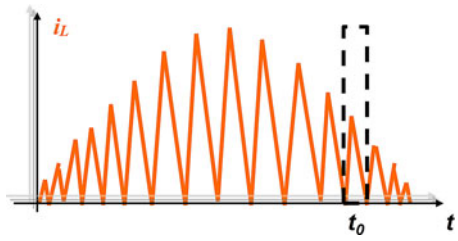

Fig. 8. Inductor current of a CRM PFC converter.

150 kHz can pass the IF; all other red bars with frequencies unequal to 150 kHz are greatly attenuated (filtered out). Following the same principle, the triangular ripple currents with the frequencies adjacent to 50, 75, and 150 kHz contribute to the noise close to 150 kHz. The blue bars in Fig. 7 demonstrate this. As long as these blue bars are in the RBW, the corresponding fundamental and harmonic components will still pass the IF with limited attenuations. All other blue bars will be filtered out. In the time domain, all of these "survived" bars represent sinusoidal waveforms with frequencies equal to or close to 150 kHz and their amplitudes are equal to the height of the bars. The envelope of these sinusoidal waveforms will be recorded by the envelope detector and finally fed to the quasi-peak detector. The output of the quasi-peak detector will be determined by the envelope series in Fig. 7. Essentially, the proposed mathematical model for the quasi-peak EMI noise prediction of variable frequency noise is based on this principle, and the complete theoretical calculation is shown in Section III.

III. Quasi-Peak DM Noise Prediction

The typical inductor current waveform and input voltage waveform for a CRM PFC converter in a half line cycle is shown in Fig. 8. The peak inductor current $i_{\rm LP}(t)$ is

$$i_{\rm LP}(t) = \frac{V_{\rm in}(t)}{L_B} T_{\rm on}. \tag{4}$$

If unit power factor is achieved, the input average current $i_{\rm in}(t)$ is

$$i_{\rm in}(t) = \sqrt{2}\frac{P_{\rm in}}{V_{\rm rms}}\sin(\omega t) = \frac{1}{2} i_{\rm LP}(t). \tag{5}$$

From (4) and (5), the turn-on time $T_{\rm on}$ is

$$T_{\rm on} = \frac{2P_{\rm in}L_B}{V_{\rm rms}^2} = \frac{2P_o L_B}{\eta V_{\rm rms}^2}. \tag{6}$$

Thus, $T_{\rm on}$ is a constant time for the given input line voltage and load.

In a CRM PFC converter, the switching frequency varies over a half line cycle. When the circuit operates at CRM, the switching frequency $f_s(t)$ is

$$f_s(t) = \frac{1}{T_s(t)} = \frac{1 - V_{\rm in}(t)/V_o}{T_{\rm on}} = \frac{1 - \sqrt{2}V_{\rm rms}\sin(\omega t)/V_o}{T_{\rm on}}. \tag{7}$$

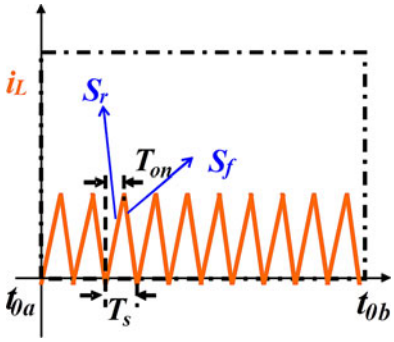

Fig. 9. The current waveform zoomed in at t_0 in Fig.7.

Thus, the minimum and maximum switching frequencies are

$$f_{s\_\min} = \frac{1 - \sqrt{2}V_{\rm rms}/V_o}{T_{\rm on}} \text{ and } f_{s\_\max} = \frac{1}{T_{\rm on}}. \quad (8)$$

However, based on the quasi-steady-state assumption, within a very short time interval, the PFC converter is like a boost converter with constant input voltage. Thus, the inductor current ripple is approximately a periodical triangular waveform during the small time interval. The inductor waveform is redrawn and zoomed in Fig. 9.

In Fig. 9, the rising slope of the ripple current is

$$S_r = \frac{V_{\rm in}(t)}{L_B} = \left(1 - \frac{T_{\rm on}}{T_s\,(t)}\right)\frac{V_o}{L_B}. \quad (9)$$

And the falling slope of the ripple current is

$$S_f = \frac{V_o - V_{\rm in}(t)}{L_B} = \frac{T_{\rm on}}{T_s\,(t)}\frac{V_o}{L_B}. \quad (10)$$

Then the ripple current in a switching cycle can be expressed as (11) shown at the bottom of this page. The amplitude of the harmonic current can be derived with Fourier analysis as

$$|i_k(f_s(t))| = \frac{1}{k^2}\frac{V_o}{L_B}\frac{1}{2\pi^2 f_s(t)}|e^{-jk2\pi f_s(t)T_{\rm on}} - 1| \quad (12)$$

where k is the order number and $k = 1,2,3\ldots$.

Equation (12) is the expression for the noise source current of CRM PFC converters.

In CRM PFC applications, conducted EMI standards are from 150 kHz to 30 MHz. To measure the EMI noise, $f_{\rm IF}$ of the spectrum analyzer sweeps from 150 kHz to 30 MHz. The EMI measurement setup is shown in Fig. 10.

In Fig. 10, the input impedance of a spectrum analyzer is equivalent to a 50 Ω resistance. The noise separator [15] is used to separate the DM noise from the CM noise. (It can also be set up to measure the CM noise.) The noise separator maintains a 50 Ω input impedance (from each line to the ground) within the measured frequency range. The principle and the mathematical

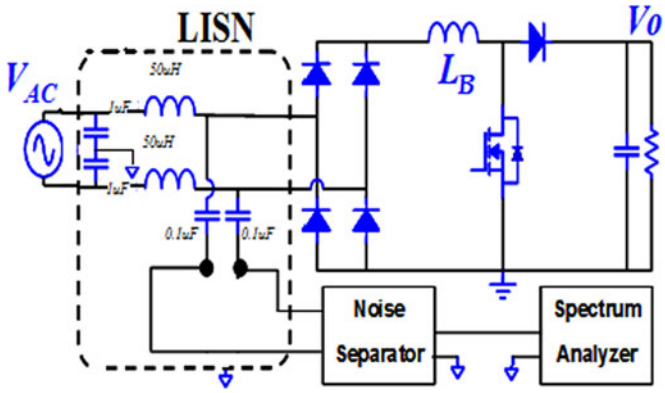

Fig. 10. EMI measurement setup (without input capacitors after the diode bridge).

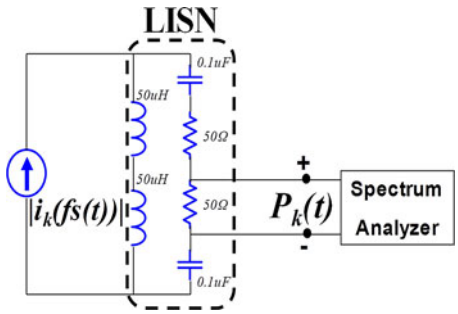

Fig. 11. Simplified circuit for DM noise measurement.

model of the noise separator are fully described in [15]. The impedances of two 1 μF capacitors are ignored; thus, the DM equivalent circuit of Fig. 10 can be simplified to the circuit in Fig. 11.

In Fig. 11, the gain of the LISN is

$$G_{\rm LISN}(f) = \left|\frac{R_{\rm LISN}\cdot 2\cdot j\,(2\pi f)\,L_{\rm LISN}}{2R_{\rm LISN} + (2/j\,(2\pi f)\,C_{\rm LISN}) + 2\cdot j\,(2\pi f)\,L_{\rm LISN}}\right| \quad (13)$$

where $R_{\rm LISN} = 50\ \Omega$, $L_{\rm LISN} = 50\ \mu$H, and $C_{\rm LISN} = 0.1\ \mu$F.

So the noise added to the input of the spectrum analyzer is

$$P_k(t) = |i_k(f_s(t))||G_{\rm LISN}\,(kf_s(t))\,| \quad (14)$$

where k is the harmonic order number and $k = 1,2,3\ldots$.

For each order harmonic, the envelope is

$$E_k\,(t, f_{\rm IF}) = P_k\,(t)\,|G_{\rm IF}\,(kf_s(t), f_{\rm IF})\,|. \quad (15)$$

$$i_{rp}(\tau) = \begin{cases} S_r\cdot\tau - \dfrac{1}{2}S_r\cdot T_{\rm on} = \dfrac{V_o}{L_B}\left(1 - \dfrac{T_{\rm on}}{T_s\,(t)}\right)\tau - \dfrac{1}{2}\dfrac{V_o}{L_B}\left(1 - \dfrac{T_{\rm on}}{T_s\,(t)}\right)T_{\rm on} & 0 \le \tau < T_{\rm on} \\ \dfrac{1}{2}S_r\cdot T_{\rm on} - S_f\cdot(\tau - T_{\rm on}) = -\dfrac{V_o}{L_B}\dfrac{T_{\rm on}}{T_s\,(t)}\tau + \dfrac{1}{2}\dfrac{V_o}{L_B}\left(1 + \dfrac{T_{\rm on}}{T_s\,(t)}\right)T_{\rm on} & T_{\rm on} \le \tau < T_s\,(t)\,. \end{cases} \quad (11)$$

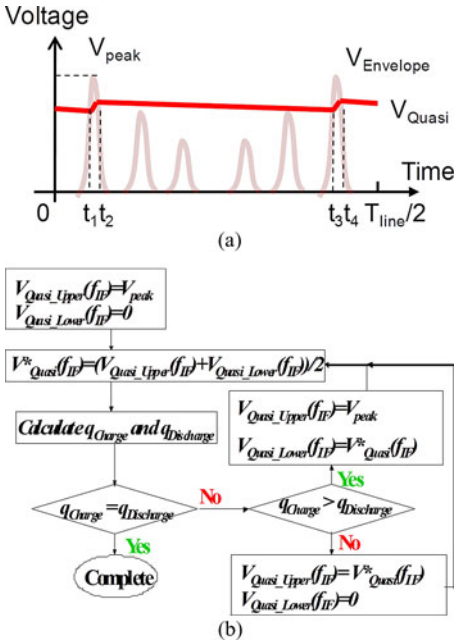

Fig. 12. Principle of a quasi-peak detector. (a) Charge balance. (b) Dichotomy algorithm for calculation.

The output of the envelope detector can be described as

$$E\left(t, f_{\mathrm{IF}}\right) = \max\left\{E_1\left(t, f_{\mathrm{IF}}\right), E_2\left(t, f_{\mathrm{IF}}\right), ..., E_N\left(t, f_{\mathrm{IF}}\right)\right\} \tag{16}$$

where $N = [f_{\mathrm{IF}} / \min f_s]$, which is the largest integer smaller than $f_{\mathrm{IF}} / \min f_s$.

The output of the envelope detector is fed to a quasi-peak detector for quasi-peak noise measurement. Because the quasi-peak detector's charge time constant is much smaller than its discharge time constant, at the beginning, the voltage across the output capacitor is charged up by $E(t, f_{\mathrm{IF}})$ and finally reaches a steady state. In Fig. 12, at steady state, during the time intervals t_1–t_2 and t_3–t_4, the envelope voltage V_{Envelope} is higher than the quasi-peak voltage V_{Quasi}; the capacitor in the quasi-peak detector is charged up. The charges injected in intervals t_1–t_2 and t_3–t_4 are equal. On the other hand, during the whole time period 0–(T_{line}/2), where T_{line} is the period of the line current, the capacitor in the quasi-peak detector is discharged. Applying the charge balance principle on the capacitor, at steady state, (17) holds. For noise at each given frequency f_{IF}, the quasi-peak noise value $V_{\mathrm{quasi}}(f_{\mathrm{IF}})$ can be calculated numerically using the dichotomy algorithm based on the charge balance principle described in Fig. 12 and

$$2\int_{t_1}^{t_2}\left(\frac{V_{\mathrm{Envelope}} - V_{\mathrm{Quasi}}}{R_1}\right)dt = \frac{V_{\mathrm{Quasi}}}{R_2}\frac{T_{\mathrm{line}}}{2}. \tag{17}$$

The quasi-peak detector is actually a charge–discharge network, with charging time constant much smaller than discharging time constant. Thus, the output of the quasi-peak detector will be gradually charged up by the input noise envelope signal. However, the output can never be larger than the peak value of the input envelope signal. So, we can initialize the output $V^*_{\mathrm{Quasi}}(f_{\mathrm{IF}})$ with half of the peak value of the input envelope signal. If this initial value is equal to the final steady state value of the output, then (17) should be satisfied. If not, then we could adjust the initial value by dichotomy, according to the relationship between charge and discharge in (17). Finally, the steady state value could be obtained in several iterations. The dichotomy algorithm is shown in Fig. 12(b). In Fig. 12(b), $V_{\mathrm{Quasi\_Upper}}(f_{\mathrm{IF}})$ and $V_{\mathrm{Quasi\_Lower}}(f_{\mathrm{IF}})$ are the upper limit and lower limit of the output of the quasi-peak detector, respectively. V_{peak} is the peak value of the input envelop signal. q_{Charge} and $q_{\mathrm{Discharge}}$ are the charges in charging and discharging processes, respectively. The detailed math calculation is not shown here.

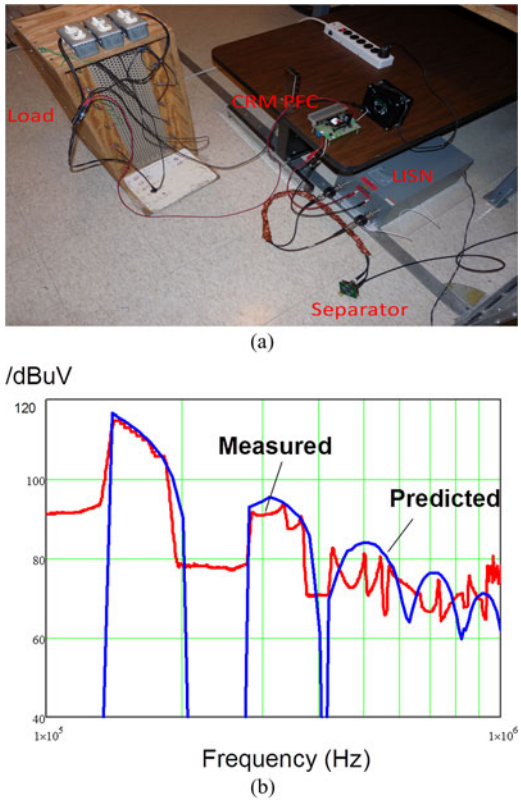

Fig. 13. EMI measurement for a CRM PFC converter. (a) Measurement setup. (b) Comparison of the measured and calculated quasi-peak noise.

The output of the quasi-peak detector within the whole noise spectrum can be obtained by sweeping f_{IF} from 150 kHz to 30 MHz. However, when the frequency is above several megahertz, the circuit parasitic parameter such as the equivalent parallel capacitance of the boost inductor will play an important role [17] to weaken the accuracy of the prediction. In this paper, only noise at low frequency (LF) range from 150 kHz to 1 MHz is considered because LF noise determines the filter inductance and capacitance [16].

A CRM PFC converter [18] is first tested to verify the mathematical model and the proposed quasi-peak DM noise prediction technique. The measurement setup is shown in Fig. 13(a). The input RMS voltage V_{RMS} is 110 V, the output voltage V_o is 400 V, the boost inductor L_B is 130 μH, and the output power P_o is 160 W. The comparison between the measured and calculated

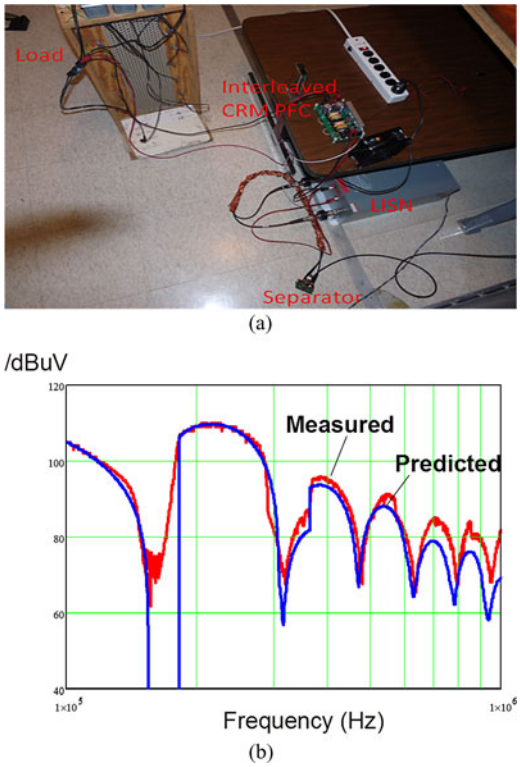

Fig. 14. EMI measurement for an interleaved CRM PFC converter. (a) Measurement setup. (b) Comparison of the measured and calculated quasi-peak noise.

results is shown in Fig. 13(b). It is shown that the experimental result verifies the predicted result.

In the second step, the proposed mathematical model and the quasi-peak DM noise prediction technique are applied to a two-phase interleaved CRM PFC converter [19] ($V_{\rm RMS} = 120$ V, $P_o = 600$ W, $L_B = 140$ μH, $V_o = 400$ V). The measurement setup is shown in Fig. 14(a). The EMI is measured to verify the predicted result in Fig. 14(b). In Fig. 14(b), LF noise, which is important for EMI filter design, is accurately predicted.

IV. Analysis of the Worst DM Noise Case

In Fig. 2, for a CRM PFC converter, both the highest and the lowest switching frequencies are shown with the highest input voltage. This indicates that the highest input voltage causes the widest frequency range. For a traditional constant frequency PFC converter, the input voltage has no influence on the switching frequency. So generally, the worst DM EMI case for a constant frequency PFC converter would be at low line and full load, because under such conditions, the PFC converter has the largest input current ripple. However, the same result does not apply to CRM PFC converters because their switching frequencies are determined by both the input voltage and the load. Because of this, it is very necessary to do worst case analysis for the sake of DM EMI filter design.

It should be pointed out that although the highest input voltage leads to the lowest switching frequency, only noise with a frequency above 150 kHz is of concern because the EMI standards start from 150 kHz. For example, if the lowest switching

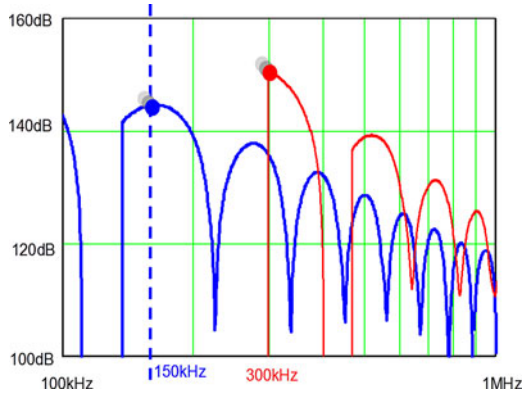

Fig. 15. Comparison of the predicted quasi-peak noise.

frequency is 30 kHz, only the harmonics with an order equal to or higher than 5 need to be attenuated. On the other hand, at some lower input voltages, the converter may generate an input current ripple with a frequency equal to 150 kHz. Although the amplitude of this current ripple is smaller than that with 30 kHz frequency, the fundamental of 150 kHz ripple is higher than the fifth-order harmonic of the 30 kHz current ripple. Because of this, the noise within the whole input voltage and load ranges should be investigated to find the worst EMI. After the worst case is identified, the EMI filter can be designed.

Since the DM EMI noise of a CRM PFC converter can be accurately predicted in previous sections, the worst DM EMI noise case can be predicted and analyzed.

The question is how to define the worst case for the EMI noise. The worst case should be the one that requires the biggest EMI filter. Because of this, we cannot consider an EMI noise spectrum with the highest noise peak as the worst case because another EMI noise spectrum with a lower noise peak at a lower frequency may require a bigger EMI filter. An example is illuminated in Fig. 15. Two predicted quasi-peak noise spectra are shown in Fig. 15. One has a noise peak of 150 dB at 300 kHz and the other has a noise peak of 143 dB (lower noise peak) at 150 kHz (lower frequency). If a simple *LC* filter is used to attenuate the EMI noise, considering that the insertion gain of the *LC* filter is increasing by 40 dB/decade after the corner frequency, the filter's corner frequency for these two noise spectra can be calculated using [24]

$$f_{\rm DM} = \frac{f_{\rm Noise}}{10^{\rm Attenuation/40}}. \tag{18}$$

The calculated corner frequencies are 2.38 and 1.78 kH, respectively. It turns out that the latter needs a larger *LC* filter. It is also clear that the corner frequency is a great criterion to evaluate the size of *LC* filters. Even for real EMI filter designs, the corner frequency criterion would be still valid to evaluate the size of EMI filters with different filter topologies. Because of this, the worst case of the DM EMI noise is the one requiring the lowest DM filter corner frequency.

A two-stage π-type filter is used in Fig. 16 for analysis. Considering that the insertion gain of the two-stage filter (CLCLC) is increasing by 100dB/decade after the corner frequency, the

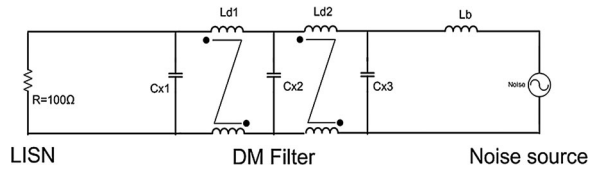

Fig. 16. Two-stage π-type DM EMI filter.

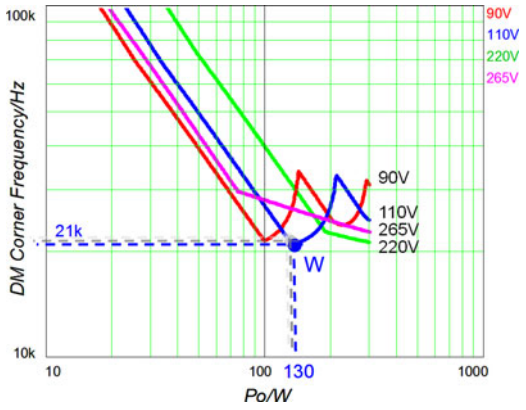

Fig. 17. DM filter corner frequency f_{DM} versus load P_o.

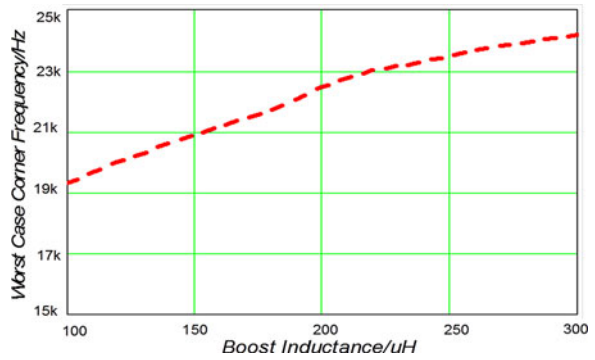

Fig. 18. Worst DM corner frequency versus boost inductance.

filter's corner frequency for the given noise spectra can be calculated using

$$f_{\mathrm{DM}} = \frac{f_{\mathrm{Noise}}}{10^{\mathrm{Attenuation}/100}}. \tag{19}$$

For a design at the given boost inductance, the quasi-peak DM EMI noise with certain input line voltage and certain load can be predicted with the method proposed previously. The DM filter's corner frequency f_{DM} can be calculated based on the predicted noise and the EMI standard. The process is repeated for the whole load range with the input line voltage as a sweeping parameter. The curves of DM filter's corner frequency versus load can be obtained via this process. The calculated curves for a 300-W CRM PFC converter with $L_B = 150\ \mu$H are shown in Fig, 17. From these curves, the worst case, $f_{\mathrm{DM}} = 21$ kHz at 150 kHz, is at 110 V low line and partial load. This is not the same as the case of constant frequency CCM PFC converters, where the worst case is generally at 90 V low line and full load.

The EMI filter can be designed based on the analyzed worst case. The design procedure is referred to [16], [20]–[23].

The worst DM filter corner frequency as a function of boost inductance can be further developed in Fig. 18. For different boost inductance, the DM EMI filter can be efficiently designed with predicted noise without noise measurement, which is usually impossible before the hardware is finished.

V. Conclusion

In this paper, the mathematical model for quasi-peak DM noise detection is developed. The DM EMI noise of CRM PFC converters is predicted with the proposed technique. The experimental results prove the effectiveness of the proposed technique up to 1 MHz. The worst DM noise case can be identified based on the predicted DM noise. The proposed technique can help avoid overdesign of the EMI filters in CRM PFC converters. The predicted corner frequency–boost inductance curves could help predesign of EMI filters without noise measurement. It is expected that this technique can help engineers optimize the boost inductor design with respect to the tradeoff between efficiency and the total size of boost inductors and DM EMI filters.

References

[1] [Online]. Available: http://www.energystar.gov/
[2] J. Sun, "Light load efficiency improvement for laptop VRs," in *Proc. Appl. Power Electr. Conf.*, 2007, pp. 120–126.
[3] S. Wang, "Common-mode noise reduction for power factor correction circuit with parasitic capacitance cancellation," *IEEE. Trans. Electromagn. Compat.*, vol. 49, no. 3, pp. 537–542, Aug. 2007.
[4] S. Wang, "Common mode noise reduction for boost converters using general balance technique," *IEEE Trans. Power Electron.*, vol. 22, no. 4, pp. 1410–1416, Jul. 2007.
[5] P. Kong, "Common mode EMI noise suppression for bridgeless PFC converters," *IEEE Trans. Power Electron.*, vol. 23, no. 1, pp. 291–297, Jan. 2008.
[6] L. Yang, "Modeling and characterization of a 1 KW CCM PFC converter for conducted EMI prediction," in *Proc. Appl. Power Electr. Conf.*, 2004, pp. 763–769.
[7] S. Brehaut, "Analysis EMI of a PFC on the band-pass 150 kHz–30 MHz for a reduction of the electromagnetic pollution," in *Proc. Appl. Power. Electr. Conf.*, 2004, pp. 695–700.
[8] C. Wang, "EMI study for the interleaved multi-channel PFC," in *Proc. Power Electr. Spec. Conf.*, 2007, pp. 1336–1342.
[9] F. Lin, "Reduction of power supply EMI emission by switching frequency modulation," *IEEE Trans. Power Electron.*, vol. 9, no. 1, pp. 132–137, Jan. 1994.
[10] R. Morrison, "The effect of switching frequency modulation on the differential-mode conducted interference of the boost power-factor correction converter," *IEEE Trans. Electromagn. Compat.*, vol. 49, no. 3, pp. 526–536, Aug. 2007.
[11] *Limits and Methods of Measurement of Radio Disturbance Characteristics of Information Technology Equipment,* European Norm Standard EN55022, 1994.
[12] *Specification for Radio Disturbance and Immunity Measuring Apparatus and Methods: Part 1-2. Radio Disturbance and Immunity Measuring Apparatus—Ancillary Equipment—Conducted Disturbances,* IEC CISPR 16-1-2, Jan. 2009.
[13] Agilent *Spectrum Analysis Basics* Agilent Appl. Note AN150.
[14] F. Krug, "Quasi-peak detector model for a time-domain measurement system," *IEEE Trans. Electromagn. Compat.*, vol. 47, no. 2, pp. 320–326, May 2005.
[15] S. Wang, "Characterization, evaluation, and design of noise separator for conducted EMI noise diagnosis," *IEEE Trans. Power Electron.*, vol. 20, no. 4, pp. 974–982, Jul. 2005.
[16] F.-Y. Shih, "A procedure for designing EMI filters for AC line applications," *IEEE Trans. Power Electron.*, vol. 11, no. 1, pp. 170–181, Jan. 1996.
[17] S. Wang, F. C. Lee, and W. G. Odendaal, "Single layer iron powder core inductor model and its effects on boost PFC EMI noise," in *Proc. IEEE Power Electron. Spec. Conf.*, Jun.15–19, 2003, vol. 2, pp. 847–852.

[18] STMicroelectronics, *Advanced Transition-Mode PFC Controller* Datasheet L6563.
[19] Texas Instruments, *UCC28060 Natural Interleaving™ dual-phase transition-mode PFC controller* [Online]. Available: http://focus.ti.com/lit/ds/slus767e/slus767e.pdf 2012.
[20] A. A. Fardoun and E. H. Ismail, "Reduction of EMI in AC drives through dithering within limited switching frequency range," *IEEE Trans. Power Electron.*, vol. 24, no. 3, pp. 804–811, Mar. 2009.
[21] R. Yang, B. Zhang, D. Qiu, and Z. Liu, "Time–frequency and wavelet transforms of EMI dynamic spectrum in chaotic converter," *IEEE Trans. Power Electron.*, vol. 24, no. 4, pp. 1083–1092, Apr. 2009.
[22] S. Wang, Y. Y. Maillet, F. Wang, D. Boroyevich, and R. Burgos, "Investigation of hybrid EMI filters for common mode EMI suppression in a motor drive system," *IEEE Trans. Power Electron.*, vol. 25, no. 4, pp. 1034–1045, Apr. 2010.
[23] J. Biela, A. Wirthmueller, R. Waespe, M. L. Heldwein, K. Raggl, and J. W. Kolar, "Passive and active hybrid integrated EMI filters," *IEEE Trans. Power Electron.*, vol. 24, no. 5, pp. 1340–1349, May 2009.
[24] Y. Y. Maillet, R. Lai, S. Wang, F. Wang, R. Burgos, and D. Boroyevich, "High-density EMI filter design for DC-fed motor drives," *IEEE Trans. Power Electron.*, vol. 25, no. 5, pp. 1163–1172, May 2010.

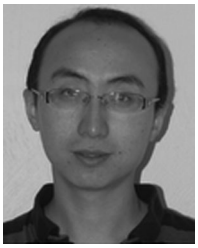

Zijian Wang received the B.S. degree from Zhejiang University, Hangzhou, China, and the M.S. degree from Virginia Polytechnic Institute and State University (Virginia Tech), Blacksburg, both in electrical engineering, in 2006 and 2010, respectively.

From 2007 to 2011, he was a Research Assistant in the Center for Power Electronics Systems, Virginia Tech. Since October 2011, he has been with the Monolithic Power Systems, Inc., San Jose, CA, as an Application Engineer focusing on the dc–dc power converters. His research interests include power factor correction converters, EMI modeling, and design optimization.

Shuo Wang (S'03–M'06–SM'07) received the Ph.D. degree from the Center for Power Electronics Systems (CPES), Virginia Polytechnic Institute and State University, (Virginia Tech), Blacksburg, in 2005.

He has been with the Department of Electrical and Computer Engineering, The University of Texas at San Antonio, San Antonio, since 2010. He was with the Electrical Power Systems Group, GE Aviation Systems, Vandalia, OH, from 2009 to 2010. From 2005 to 2009, he was with CPES at Virginia Tech. He is the holder of six U.S. patents and has one more pending. He has published approximately 90 journal and conference papers. His research interests include electromagnetic interference/electromagnetic compatibility in power electronics systems, high-density power conversion, three-phase power conversion and inversion, high power electric vehicle superfast charging, motor drives, generator control, power systems, and microgrid.

Dr. Wang is an Associate Editor of the IEEE TRANSACTIONS ON INDUSTRY APPLICATIONS. He was the recipient of the 2005 Best Transactions Paper Award from the IEEE TRANSACTIONS ON POWER ELECTRONICS and the William M. Portnoy Award at the IEEE Industry Applications Society Annual Conference in 2004. He received prestigious NSF Career Award in 2012 from National Science Foundations.

Pengju Kong (M'08) received the B.S. and Ph.D. degrees in electrical engineering from Tsinghua University, Beijing, China, in 2003 and 2009, respectively.

He was a Visiting Scholar in the Center for Power Electronics Systems (CPES), Virginia Polytechnic Institute and State University, Blacksburg, between 2005 and 2009. He continued his research at CPES as a Postdoctoral Associate after receiving the Ph.D. degree. Since 2011, he has been with Intersil Corporation, Milpitas, CA, as an Application Engineer. His research interests include EMI modeling and reduction techniques in power electronics systems, power factor correction techniques, high-frequency dc/dc converter, photovoltaic converter, and modeling and control of converters.

Fred C. Lee (S'72–M'74–SM'87–F'90) received the B.S. degree in electrical engineering from the National Cheng Kung University, Tainan, Taiwan, in 1968 and the M.S. and Ph.D. degrees in electrical engineering from Duke University, Durham, NC, in 1972 and 1974, respectively.

He is currently a University Distinguished Professor at Virginia Polytechnic Institute and State University, (Virginia Tech), Blacksburg, VA. He is the Founder and Director of the Center for Power Electronics Systems, a National Science Foundation engineering research center. He has supervised 71 Ph.D. and 80 master students at Virginia Tech. He holds 69 U.S. patents. He has authored or coauthored 238 journal articles and more than 596 refereed technical papers. His current research interests include high-frequency power conversion, distributed power systems, renewable energy, power quality, high-density electronics packaging and integration, and modeling and control.

Dr. Lee was a Recipient of the William E. Newell Power Electronics Award in 1989 and the Arthur E. Fury Award for Leadership and Innovation in 1998. From 1993 to 1994, he served as President of the IEEE Power Electronics Society. Dr. Lee was named to the National Academy of Engineering in 2011.